Journal of Sound and Vibration (1992) **153**(1), 37–50

VIBRATION TRANSMISSION THROUGH ROLLING ELEMENT BEARINGS, PART IV: STATISTICAL ENERGY ANALYSIS

T. C. LIM† AND R. SINGH

Department of Mechanical Engineering, The Ohio State University, 206 West 18th Avenue, Columbus, Ohio 43210-1107, *U.S.A.*

(*Received* 6 *December* 1989, *and accepted in revised form* 7 *January* 1991)

A theoretical coupling loss factor for the vibration transmission through a rolling element bearing problem has been developed for the statistical energy analysis (SEA) technique. This scheme includes the bearing stiffness matrix developed earlier in the companion paper Part I. The same problem has been analyzed previously by using deterministic vibration models in Parts II and III. In this paper, a new analytical procedure is developed to obtain the coupling loss factor between the shaft and casing which is based on the solution of the boundary value problem at the plate-bearing interface. Several example cases are chosen to demonstrate the salient features of this method: I, a plate-cantilevered beam problem; II, case I with circular shaft-bearing replacing the cantilevered beam; III, a shaft-bearing-plate system. Example case I is a revised version of the problem analyzed earlier by Lyon and Eichler (reference [6] of this paper). Our proposed calculation indicates an improvement in the coupling loss factor prediction for a thin plate-cantilevered beam system. Example case II deals with the development of a theoretical scheme to compute coupling loss factor for a bearing system. This development is extended further to predict mean-square vibratory response of a rectangular plate for example case III. Results of the statistical energy analysis compare well with the predictions yielded by deterministic model of Part II. Predictions for example cases I and III are found to be in good agreement with measurements.

1. INTRODUCTION

It has been shown in Parts I–III [1–3], by using classical lumped parameter and dynamic finite element (FEM) techniques, that the proposed bearing model is clearly superior to the existing simple models for predicting vibration transmission through bearings in a shaft-bearing-plate system. Although the proposed models have been shown to be reliable up to a moderately high frequency, it is conceivable that these models are inadequate at very high frequencies where the modal density tends to be high. Classical vibration models do not predict modes accurately in this frequency regime, and even if it is possible to do so by employing closely spaced nodal points, such models require a significantly large computational effort. Moreover, the vast amount of predicted response spectra at many spatial points would be difficult to interpret. Accordingly, asymptotic or statistical methods must be adopted; typical techniques include the statistical energy analysis [4–8], asymptotic modal analysis [9–11] and asymptotic analysis using infinite system impedances [12].

This study is concentrated on the development of a theoretical broadband coupling loss factor, which is a key parameter for the statistical energy analysis (SEA), of a shaft-bearing-plate system. The SEA method has been applied successfully to those structural and acoustic systems which exhibit high modal overlap and weak coupling

† Currently with Structural Dynamics Research Corporation, Milford, Ohio 45150, U.S.A.

0022-460X/92/040037+14 $03.00/0

between subsystems [4–8, 13–18]. However several unresolved research issues still exist [5, 8–10, 19, 20]. The specific objectives of this study are (i) to develop a theoretical scheme to compute a coupling loss factor for a typical rolling element bearing system, (ii) to demonstrate the applicability of SEA to the bearing problem, (iii) to analyze the following three example cases: I, a plate-cantilevered rectangular beam; II, case I with circular shaft-bearing system replacing the cantilevered beam; III, a circular shaft-bearing-plate-mount system; and finally, (iv), to perform parametric studies to examine the characteristics of vibratory energy transfer through bearings. The first and second example cases are revised and extended versions of a study performed by Lyon and Eichler [4, 6]. The final example case examines an experimental set-up which was analyzed earlier in Part II [2] by using the deterministic finite element method. Predictions yielded by each method will be compared with the experimental results.

2. LITERATURE REVIEW

A majority of publications are on the application of SEA to dynamic systems with high modal overlap and weak coupling such as structural-acoustical interactions in a fuselage [4, 13, 21], interior noise predictions [13], and vibratory energy transmission in mechanical equipment [4]. Of interest here is analytical or experimental estimation of SEA parameters for simple structural systems described by a flat plate, a cylinder and/or a shaft [4, 6, 7, 14]. In these studies, structural connections are often assumed rigid such as in the ideally welded case.

Lyon and Eichler [4, 6] in 1964 and Lyon and Scharton [7] in 1965 developed analytical expressions for the coupling loss factor η in several connected structures, such as a plate bonded to a cantilevered beam [4, 6]. Here η was derived by assuming a semi-infinite beam attached to an infinite plate and by further assuming that only a dynamic moment coupling at the joint can describe the motion/force transmission phenomenon. This problem is re-examined in this study and is then extended to a circular shaft-bearing-plate-mount system. In addition. Lyon and Eichler [4, 6] also developed SEA models of two structures inter-connected through a single (scalar) stiffness element. Typical examples include two discrete masses coupled by a linear spring, and a plate attached to a single-degree-of-freedom resonator [4]. The longitudinal vibration of linearly coupled rods was analyzed by Remington and Manning [18] in 1975. Loss factors of typical line or point connected structures such as a plate welded to a cylinder, cross-beams and two perpendicular plates bolted or welded together have been calculated assuming ideal rigid joints [4, 6, 7, 22, 23]. But a compliant bearing support problem is yet to be analyzed.

3. EXAMPLE CASE I: COUPLING LOSS FACTOR OF PLATE-CANTILEVERED BEAM SYSTEM

First, we attempt to rework the plate-cantilevered beam problem of Lyon and Eichler [4, 6] as shown in Figure 1. Only flexural motions of the rectangular plate and rectangular beam are considered in this case. Accordingly, Lyon and Eichler [4, 6] developed an expression for the coupling loss factor η_{sc} which describes the vibratory energy transfer between the beam(s) and the plate(c) due to a moment coupling at the joint,

$$\eta_{sc}(\omega) = \frac{(2\rho_s A_s \kappa_s c_s)^2}{\omega m_s} \left| \frac{Z_c}{Z_c + Z_s} \right|^2 \mathrm{Re}\left(\frac{1}{Z_c}\right), \tag{1}$$

where $\kappa_s = \sqrt{I_s/A_s}$ is the radius of gyration, $c_s = \sqrt{E/\rho_s}$ is the wave speed, m_s is the mass and Re ( ) implies the real part of a complex variable (a list of symbols is given in the

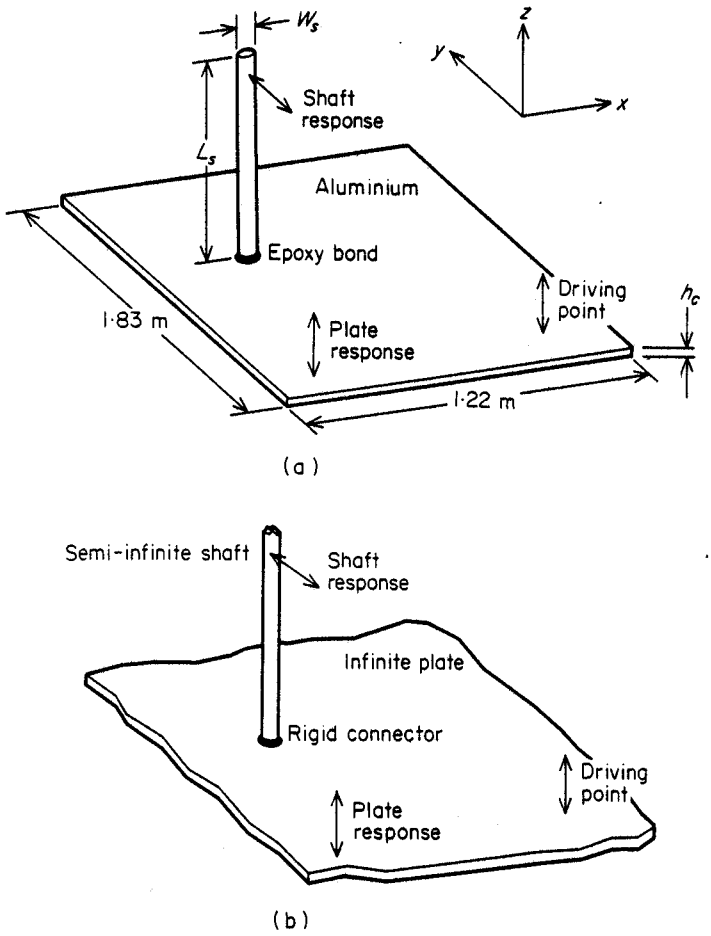

Figure 1. Schematic of example case I: a plate-cantilevered beam. (a) Experimental finite system; (b) theoretical infinite system with a small patch.

Appendix) with the sign convention $e^{+i\omega t}$, the deterministic junction moment impedances of the plate Z_c for a moment applied to a small patch, and beam Z_s are [6, 24]

$$Z_c(\omega) = \frac{16\rho_c h_c \kappa_c^2 c_c^2}{\omega[1-(4i/\pi)\ln(k_c h_s)]}, \qquad Z_s(\omega) = \frac{\rho_s A_s \kappa_s^2 c_s^2 k_s}{\omega}(1-i), \tag{2}$$

where k is the wavenumber and h is the plate or beam thickness. Here, note that Z_s of equation (2) differs from the Lyon and Eichler expression [4, 6] in the sign of the imaginary part, which is probably a typographical error. They assumed that $|Z_c| \gg |Z_s|$, $\kappa_s = \kappa_c$, $c_s = c_c$ and $\rho_s = \rho_c$, and simplified equation (1) to yield a frequency invariant expression for η_{sc} as

$$\eta_{sc} = W_s/(4L_s), \tag{3}$$

where W_s and L_s are the beam width and length, respectively, as shown in Figure 1. However, our calculations indicate that $|Z_c| > |Z_s|$ but not $|Z_c| \gg |Z_s|$ for the parameters used by Lyon and Eichler [6], as shown in Figure 2(a). By using equation (1), the frequency-averaged η_{sc} has been recomputed and is compared with the approximate model given by equation (3) in Figure 2(b). Experimental results for η_{sc} given by Lyon and Eichler [6] are also plotted in Figure 2(b). It seems that our calculation is better than the earlier prediction, even though an approximate impedance expression for a moment applied to a small patch is used. At low frequency, a discrepancy is observed between theory and experiment which is primarily due to the low modal density in this

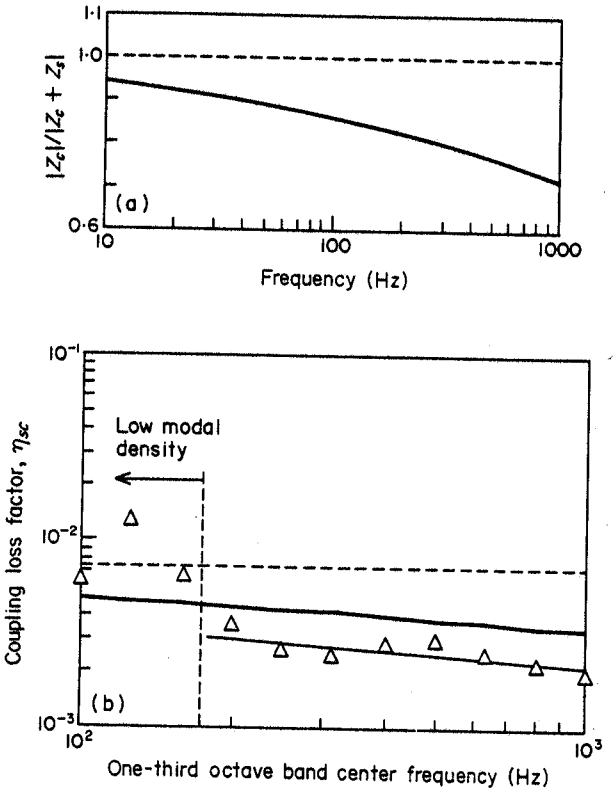

Figure 2. Comparison between the Lyon and Eichler approximation [4, 6] and our proposed formulation for example case I. (a) Comparison of $|Z_c|/|Z_c + Z_s|$; - - -, approximate model; ——, proposed. (b) Comparison of predicted η_{sc} with experimental results given by Lyon and Eichler [4, 6]; △, experiment; ——, least squares curve fit of experimental data; ——, proposed; - - -, approximate model.

regime. The presence of a low natural frequency may be due to the compliant epoxy bond between the beam and plate. However, above the threshold frequency where many modes participate, shown as a vertical line in Figure 2(b), the slope of the least squares straight line fit on the experimental data is nearly the same as the predicted η_{sc}.

4. EXAMPLE CASE II: COUPLING LOSS FACTOR OF CIRCULAR SHAFT-BEARING-PLATE SYSTEM

Next, we modify Figure 1 by inserting a ball bearing between the circular shaft (which replaces the rectangular beam in Figure 1) and the rectangular plate. Again, a semi-infinite shaft and an infinite plate are assumed. For SEA, we reduce the system to a plate subsystem and a shaft-bearing subsystem. The coupling loss factor η_{sc} is still given by equation (1), but Z_s must be modified to account for the compliant bearing.

Consider a shaft with boundary conditions shown in Figure 3. The bearing end is subjected to zero transverse velocity $v_{ysa}(t, z = 0^-) = 0$ and a sinusoidally varying moment

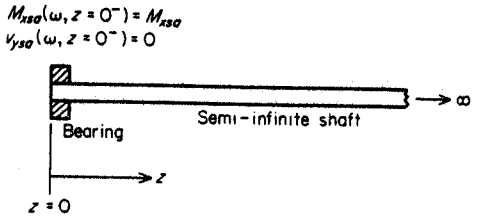

Figure 3. Boundary conditions for example case II: semi-infinite shaft-bearing system.

$M_{xsa}(t, z=0^-) = M_{xsa}\, e^{i\omega t}$. Here, $z=0^-$ refers to the junction point between bearing and plate, and $z=0^+$ is the junction point between the bearing and shaft. Next, we attempt to obtain a boundary condition at the bearing-shaft interface using the boundary condition at the plate-bearing interface. Substituting $v_{ysa}(\omega, z=0^-)=0$ into the definition of bearing force vector $\{f(\omega)\}_b = [K]_{bm}\{v)\omega)\}_b/i\omega$, where $\{v(\omega)\}_b$ and $[K]_{bm}$ are the bearing velocity vector and stiffness matrix respectively, yields

$$F_{ysa}(\omega, 0^+) = \left(\frac{k_{by\theta_x}}{k_{b\theta_x\theta_x}}\right) M_{xsa} + \frac{v_{ysa}(\omega, 0^+)}{i\omega}\left\{\left(\frac{k_{by\theta_x}}{k_{b\theta_x\theta_x}}\right)^2 k_{b\theta_x\theta_x} - k_{byy}\right\}. \tag{4}$$

The governing equations for $M_{xsa}(\omega, z)$ and $F_{ysa}(\omega, z)$ of the shaft in terms of $v_{ysa}(\omega, z)$ are

$$M_{xsa} = -(EI_s/i\omega)\, d^2v_{ysa}/dz^2, \qquad F_{ysa} = (EI_s/i\omega)\, d^3v_{ysa}/dz^3. \tag{5}$$

In general, the bounded solution for $v_{ysa}(\omega, z)$ is [25]

$$v_{ysa}(\omega, z) = \{b_1\, e^{-ik_s z} + b_2\, e^{-k_s z}\}. \tag{6}$$

Using equations (5) and (6), we enforce the boundary conditions for the shaft at $z=0^+$ to obtain the following closed form solution for the coefficient vector $\{b\}=\{b_1, b_2\}^T$:

$$b_1 = \frac{i\omega M_{xsa}}{EIk_s^2} + \frac{(\omega k_{by\theta_x}/k_{b\theta_x\theta_x}) - i\omega k_s - (\omega/EIk_s^2)(k_{byy} - k_{by\theta_x}^2/k_{b\theta_x\theta_x})}{EIk_s^3(1+i) - 2ik_{byy} + 2ik_{by\theta_x}^2/k_{b\theta_x\theta_x}} M_{xsa},$$

$$b_2 = \frac{(\omega k_{by\theta_x}/k_{b\theta_x\theta_x}) - i\omega k_s - (\omega/EIk_s^2(k_{byy} - k_{by\theta_x}^2/k_{b\theta_x\theta_x})}{EIk_s^3(1+i) - 2ik_{byy} + 2ik_{by\theta_x}^2/k_{b\theta_x\theta_x}} M_{xsa}. \tag{7}$$

Hence, the bearing-shaft impedance Z_s is then given by

$$Z_s(\omega) = \frac{M_{xsa}(\omega, 0)}{(dv_{ysa}/dz)(\omega, 0^-)} = \frac{k_{b\theta_x\theta_x}}{i\omega + \{k_{by\theta_x} v_{ysa}(\omega, 0^+) + k_{b\theta_x\theta_x}(dv_{ysa}/dz)(\omega, 0^+\}/M_{xsa}}. \tag{8}$$

Although M_{xsa} appears in equation (8), Z_s is actually independent of the magnitude of M_{xsa} since $v_{ysa}(\omega, 0^+)$ and $(dv_{ysa}/dz)(\omega, 0^+)$ are linearly proportional to M_{xsa} as well in equation (5).

By using equations (1), (7) and (8), the frequency-averaged η_{sc} has been computed for several bearings, the stiffness coefficients of which are tabulated in Table 1. These cases are compared in Figure 4 with the numerical values for shaft and plate properties such as k, κ, c and m being those used by Lyon and Eichler [4, 6] in example case I. For a

TABLE 1

Typical bearing stiffness coefficients of Figure 4 for example case II

Set	k_{byy}(N/m)	$k_{by\theta_x}$(N)	$k_{b\theta_x\theta_x}$(Nm)
A	Very compliant bearings ($k_{bij} < 1E3$)		
B	1E5	5E4	2E4
C	5E5	8E4	5E4
D	1E8	1E7	1E6
E	1E8	3E7	1E7

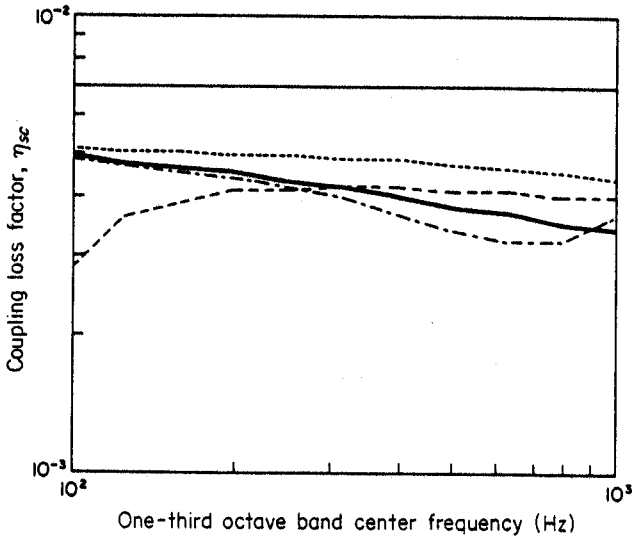

Figure 4. Coupling loss factor η_{sc} used in example case II for various bearing stiffness coefficients listed in Table 1. ——, A; - - - -, B; - · - · -, C; - - -, D; ——, E.

very soft bearing, Z_s is dominated by the bearing parameters, and hence $|Z_c| \gg |Z_s|$ is valid. This implies that η_{sc} reduces to the frequency invariant expression given by equation (3) as shown by set A in Figure 4. On the other hand, η_{sc} for a rigid bearing (say, set B or C) is typically smaller than η_{sc} given by A. The extreme values of η_{sc}, as k_{bij} or bearing preload becomes very large, depend on the relative magnitudes of the bearing stiffness coefficients, as shown in Figure 4 for sets D and E, although set E behavior occurs more frequently. Such deviation for a stiff bearing from set E is primarily due to the presence of off-diagonal stiffness coefficient such as $k_{by\theta_x}$.

5. EXAMPLE CASE III: A CIRCULAR SHAFT-BEARING-PLATE SYSTEM

5.1. THEORY

Consider another circular shaft-bearing-plate-mount system similar to example case II but with a shaft of finite length, as shown in Figure 5(a). Note that this system has been analyzed earlier in Part II [2] by using the deterministic finite element technique. Recall that the unconstrained end of the non-rotating circular shaft is subjected to a harmonically varying force $F_{ys}(t) = F_{ysa}\, e^{i\omega t} + F_{ysm}$, where F_{ysm} is the mean force. From Part II [2], we know that the longitudinal and torsional motions of the shaft and the in-plane vibration of the plate can be neglected. Hence, the shaft bending vibration and plate flexural motion are of interest here. Also, the previous deterministic vibration models indicate that the coupling between these two motions is mainly due to the dynamic moment at the bearing provided that the longitudinal shaft vibration is not excited. Accordingly, two subsystems which can be easily identified by using SEA are the transverse modes of the shaft-bearing system and the flexural modes of the plate-mount system, as shown in Figure 5(b). We now proceed to derive η_{sc} governing the vibratory energy flow between these two subsystems, using the driving point junction impedance method suggested by Lyon [4].

Since the rectangular plate dimension is much larger than the bearing dimension, the plate is again assumed infinite. Consider the vibrational power flow Π_{sc} from the shaft-bearing subsystem (subscript s) to the plate (subscript c), due to the uniform external

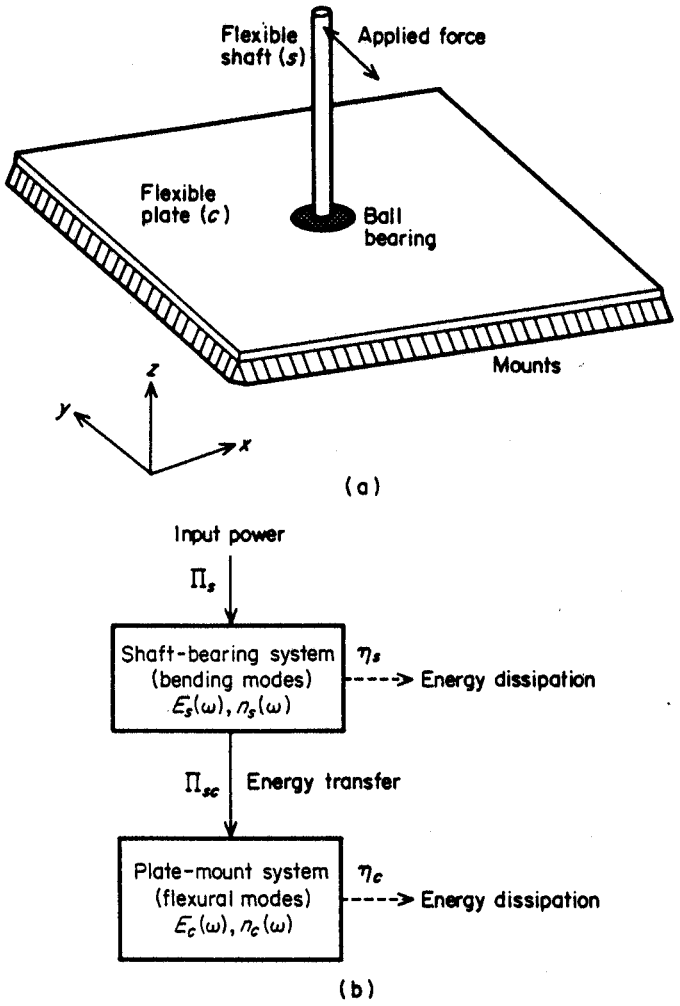

Figure 5. Example case III: (a) schematic of the circular shaft-bearing-plate-mount system described in references [2, 26] and (b) SEA model of the physical system.

Gaussian random force over a frequency bandwidth $\Delta\omega$ with center frequency ω,

$$\Pi_{sc}(\omega) = \omega\eta_{sc}(\omega)n_s(\omega)\left(\frac{E_s(\omega)}{n_s(\omega)} - \frac{E_c(\omega)}{n_c(\omega)}\right), \tag{9}$$

where n_j and E_j $(j = s, c)$ refer to subsystem modal density and total vibratory energy respectively. The modal densities per Hz of a shaft n_s and rectangular plate n_c, given for bending motion with simply supported boundary conditions [4], are

$$n_s = L_s\sqrt[4]{\rho_s\pi d_s^2/4EI_s\omega^2}, \qquad n_c = A_c/h_c\sqrt{3\rho_c(1-\mu^2)/E}, \tag{10}$$

where ρ is the material density, A_c is the plate surface area, L_s is the shaft length, E is the modulus of elasticity, I_s is the area moment of inertia of the shaft, ω is the bandwidth center frequency, h_c is the plate thickness, d_s is the shaft diameter, μ is the Poisson ratio, and the subscripts s and c denote the shaft and the plate respectively. Since the plate is assumed to be reasonably well damped and geometrically large, equation (9) is approximated assuming $n_c \gg n_s$ or $E_c/n_c \ll E_s/n_s$ to yield

$$\eta_{sc}(\omega) \approx \Pi_{sc}(\omega)/\omega E_s(\omega). \tag{11}$$

For the shaft, $E_s = m_s\langle V_s^2\rangle$, where m_s is the shaft mass and $\langle V_s^2\rangle$ is mean square shaft

transverse velocity averaged over $\Delta\omega$ and shaft length L_s. Using the expression for Π_{sc} given by Lyon and Eichler [6] as discussed in the previous section gives a frequency-averaged η_{sc} in terms of the deterministic Z_s and Z_c which is identical to that of equation (1), and which is rewritten here for the circular shaft case as

$$\eta_{sc}(\omega) = (4EI_s/\omega L_s)\,\mathrm{Re}\,(1/Z_c)|Z_c/(Z_c+Z_s)|^2. \tag{12}$$

For an infinite steel plate of thickness h_c, the point moment impedance Z_c is given in reference [25] as

$$Z_c(\omega) = \{4Eh_c^3/3\omega(1-\mu^2)\}\{1-(4\mathrm{i}/\pi)\ln(\tfrac{9}{20}k_c d_s)\}^{-1}, \qquad k_c d_s \ll 1. \tag{13}$$

The shaft-bearing impedance Z_s in equation (12) is derived next by solving the boundary value problem for the system shown in Figure 6(a). The free end of the shaft has a vanishing dynamic shear force $F_{ysa}(\omega, z = L_s) = 0$ and bending moment $M_{xsa}(\omega, z = L_s) = 0$. The bearing end is similar to that shown in Figure 3. Following the same argument used previously for example case II will lead to the two boundary conditions for the shaft described by $M_{xsa}(\omega, z = 0^+) = M_{xsa}$ and $F_{xsa}(\omega, z = 0^+) = (k_{bx\theta_y}/k_{b\theta_y\theta_y})M_{ysa} + v_{ysa}(\omega, 0^+)\ \{(k_{bx\theta_y}/k_{b\theta_y\theta_y})^2 k_{b\theta_y\theta_y} - k_{bxx}\}/(\mathrm{i}\omega)$. Governing equations are still given by equation (5), but the solution for $v_{ysa}(\omega, z)$ is assumed to be of the following form [25]:

$$v_{ysa}(t, z) = \{b_1\,\mathrm{e}^{-\mathrm{i}k_s z} + b_2\,\mathrm{e}^{\mathrm{i}k_s z} + b_3\,\mathrm{e}^{-k_s z} + b_4\,\mathrm{e}^{k_s z}\}. \tag{14}$$

Upon using equations (5) and (14), the boundary conditions yield the following algebraic problem

$$[B]\{b\} = M_{ysa}\{k_{by\theta_x}/k_{b\theta_x\theta_x},\ \mathrm{i}\omega/(EIk_s^2),\ 0,\ 0\}^{\mathrm{T}}. \tag{15}$$

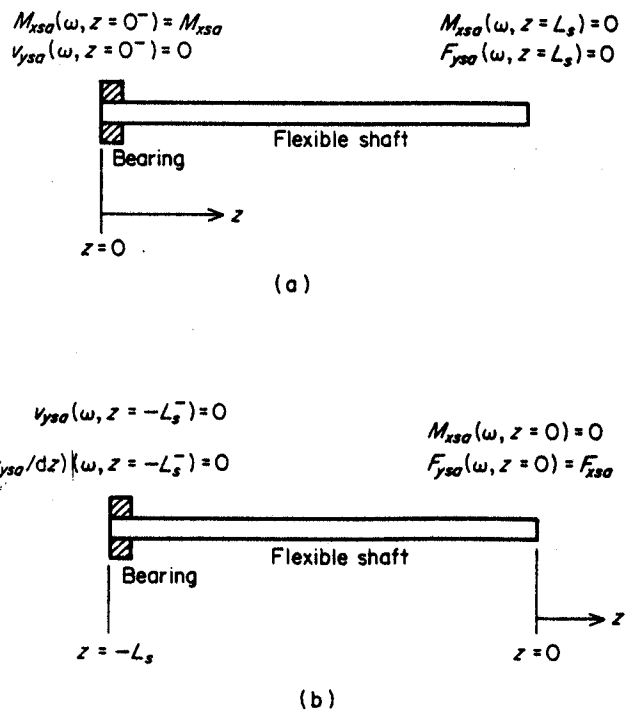

Figure 6. Boundary conditions for example case III: finite shaft-bearing system. (a) Moment applied at the bearing end; (b) force applied to the unconstrained end.

The non-zero elements of coefficient matrix $[B]$ of dimension 4 are

$$B_{11}=\frac{1}{\omega}\left(EIk_s^3-\mathrm{i}k_{byy}+\frac{\mathrm{i}k_{by\theta_x}^2}{k_{b\theta_x\theta_x}}\right),\qquad B_{12}=\frac{1}{\omega}\left(-EIk_s^3-\mathrm{i}k_{byy}+\frac{\mathrm{i}k_{by\theta_x}^2}{k_{b\theta_x\theta_x}}\right),$$

$$B_{13}=\frac{\mathrm{i}}{\omega}\left(EIk_s^3-k_{byy}+\frac{k_{by\theta_x}^2}{k_{b\theta_x\theta_x}}\right),\qquad B_{14}=\frac{\mathrm{i}}{\omega}\left(-EIk_s^3-k_{byy}+\frac{k_{by\theta_x}^2}{k_{b\theta_x\theta_x}}\right),$$

$$B_{21}=B_{22}=-B_{23}=-B_{24}=1,\qquad B_{31}=-\mathrm{i}B_{41}=\mathrm{i}\,\mathrm{e}^{-\mathrm{i}k_sL_s},\qquad B_{32}=\mathrm{i}B_{42}=-\mathrm{i}\,\mathrm{e}^{\mathrm{i}k_sL_s},$$

$$B_{33}=-B_{43}=-\mathrm{e}^{-k_sL_s},\qquad B_{34}=B_{44}=\mathrm{e}^{k_sL_s}. \tag{16}$$

Both $[B]$ and $\{b\}=\{b_1, b_2, b_3, b_4\}^{\mathrm{T}}$ can be easily obtained numerically. The bearing-shaft impedance Z_s is still given by equation (8).

The same procedure may be applied to obtain the driving point force impedance for a harmonically varying transverse force $F_{ysa}(t, z=0)$. Note that the origin is redefined at the forcing point, as shown in Figure 6(b) for convenience. The boundary conditions are $F_{ysa}(\omega, z=0)=F_{ysa}$, $M_{xsa}(\omega, z=0)=0$, $v_{ysa}(\omega, z=-L_s^-)=0$ and $(\mathrm{d}v_{ysa}/\mathrm{d}z)(\omega, -L_s^-)=0$. In a manner similar to that of the previous analysis, one obtains

$$M_{xsa}(\omega, z=-L_s)=-\{k_{b\theta_x\theta_x}\,\mathrm{d}v_{ysa}/\mathrm{d}z)(\omega, -L_s^+)+k_{by\theta_x}v_{ysa}(\omega, -L_s^+)\}/(\mathrm{i}\omega),$$

$$F_{ysa}(\omega, z=-L_s)=-\{k_{by\theta_x}(\mathrm{d}v_{ysa}/\mathrm{d}x)(\omega, -L_s^+)+k_{byy}v_{ysa}(\omega, -L_s^+)\}/(\mathrm{i}\omega). \tag{17}$$

These prescribed boundary conditions again yield a set of algebraic problem similar to equation (15). The non-zero elements of the coefficient matrix $[B]$ of dimension 4 are

$$B_{11}=-B_{21}=B_{12}=B_{22}=-B_{13}=\mathrm{i}B_{23}=-B_{14}=-\mathrm{i}B_{24}=-1\cdot 0,$$

$$B_{31}=(-\mathrm{i}k_sk_{b\theta_x\theta_x}+k_{by\theta_x}+EIk_s^2)\,\mathrm{e}^{\mathrm{i}k_sL_s},\qquad B_{32}=(\mathrm{i}k_sk_{b\theta_x\theta_x}+k_{by\theta_x}+EIk_s^2)\,\mathrm{e}^{-\mathrm{i}k_sL_s},$$

$$B_{33}=(-k_sk_{b\theta_x\theta_x}+k_{by\theta_x}-EIk_s^2)\,\mathrm{e}^{k_sL_s},\qquad B_{34}=(k_sk_{b\theta_x\theta_x}+k_{by\theta_x}-EIk_s^2)\,\mathrm{e}^{-k_sL_s},$$

$$B_{41}=(\mathrm{i}k_sk_{by\theta_x}-k_{byy}-\mathrm{i}EIk_s^3)\,\mathrm{e}^{\mathrm{i}k_sL_s},\qquad B_{42}=(-\mathrm{i}k_sk_{by\theta_x}-k_{byy}+\mathrm{i}EIk_s^3)\,\mathrm{e}^{-\mathrm{i}k_sL_s},$$

$$B_{43}=(k_sk_{by\theta_x}-k_{byy}+EIk_s^3)\,\mathrm{e}^{k_sL_s},\qquad B_{44}=(-k_sk_{by\theta_x}-k_{byy}-EIk_s^3)\,\mathrm{e}^{-k_sL_s}. \tag{18}$$

The right-hand side vector $\{b\}$ of the algebraic problem is $\{0, F_{ysa}\omega/(EIk_s^3), 0, 0\}^{\mathrm{T}}$. The force impedance at the driving point is then given by $Z_f(\omega, z=0)=F_{ysa}/v_{ysa}(\omega, 0)$. Accordingly, the input power is $\Pi_s=(1/2)F_{ysa}^2\,\mathrm{Re}\{(1/Z_f)^*\}$ where Re $\{\ \}$ is the real part of the complex variable and $(\ )^*$ implies complex conjugation.

We can now compute the vibratory energy transfer Π_{sc} through the bearing and the steady state subsystem energy levels E_s and E_c by applying the energy balances to both subsystems shown in Figure 5(b); here $\eta_{cs}=\eta_{sc}n_s/n_c$:

$$\begin{bmatrix}\eta_s+\eta_{sc}(\omega) & -\eta_{cs}(\omega)\\ -\eta_{sc}(\omega) & \eta_c+\eta_{cs}(\omega)\end{bmatrix}\begin{Bmatrix}E_s(\omega)\\ E_c(\omega)\end{Bmatrix}=\begin{Bmatrix}\Pi_s/\omega\\ 0\end{Bmatrix}, \tag{19}$$

$$E_s(\omega)=\frac{\Pi_s(\eta_c+\eta_{cs})}{\omega(\eta_s\eta_c+\eta_c\eta_{sc}+\eta_s\eta_{cs})},\qquad E_c(\omega)=\frac{\Pi_s\eta_{sc}}{\omega(\eta_s\eta_c+\eta_c\eta_{sc}+\eta_s\eta_{cs})}. \tag{20}$$

Since $E=m\langle V^2\rangle$, the following velocity levels may be obtained at any center frequency

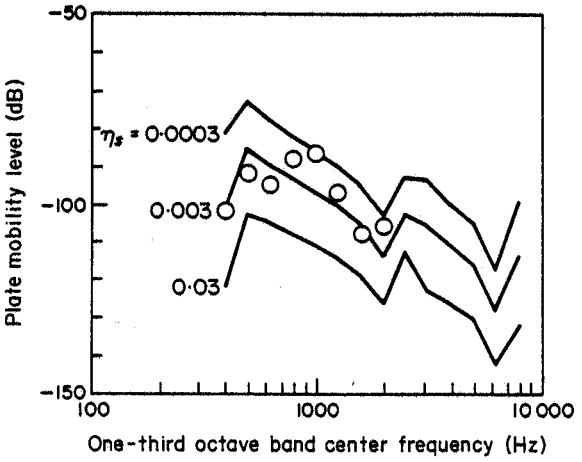

Figure 7. Compariosn between theory (——) and experiment [26] (○) for example case III with a finite shaft. Here plate mobility level in dB is $10 \log_{10} \langle V_c^2 \rangle$ *re* $\langle V_c^2 \rangle = 1{\cdot}0\ (\mathrm{m/s})^2$ for $F_{ysa} = 1{\cdot}0$ N.

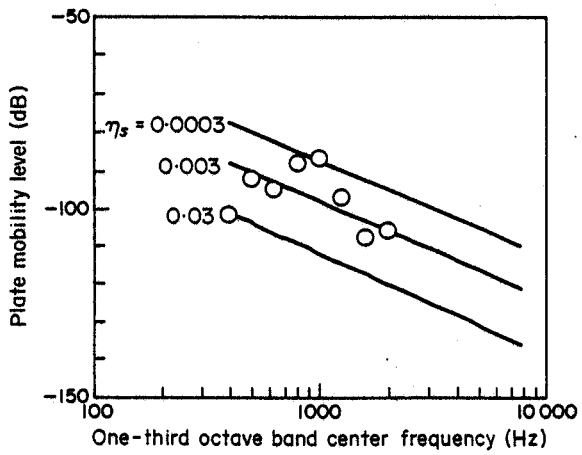

Figure 8. Comparison between theory (——) and experiment [26] (○) for example case III. Here theory is for a semi-infinite shaft.

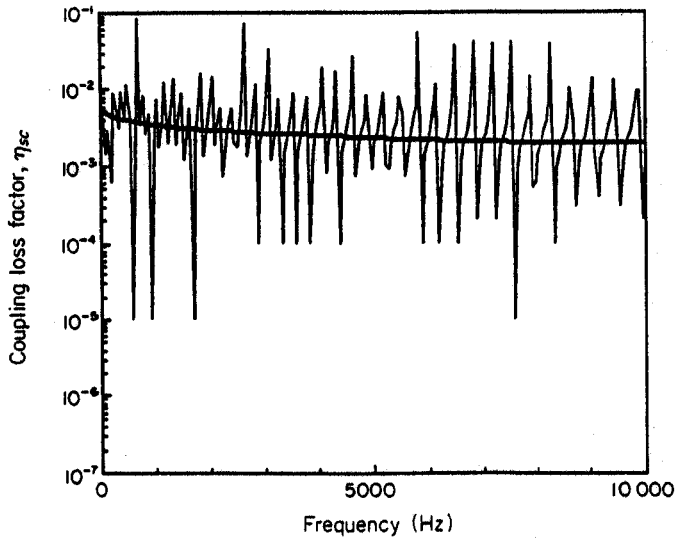

Figure 9. Predicted coupling loss factor η_{sc} for a semi-infinite (——) and a finite shaft (——) shaft in example case III.

ω from either equation (19) or (20):

$$\langle V_c^2\rangle/\langle V_s^2\rangle = (m_s/m_c)\left(\frac{\eta_{sc}(\omega)}{\{\eta_c+\eta_{cs}(\omega)\}}\right). \tag{21}$$

5.2. VALIDATION AND PARAMETRIC STUDIES

In order to validate our SEA formulation, we compare the mean square mobility level of the plate with experimental data provided by reference [26] as reported earlier in Part II [2]. Note that although all non-zero bearing stiffness coefficients k_{bij} were computed and given in Part II [2], only $k_{byy}=3{\cdot}69\text{E}8$, $k_{by\theta_x}=3{\cdot}52\text{E}5$ and $k_{b\theta_x\theta_x}=4{\cdot}19\text{E}4$ are used as they appear to be the most significant ones according to the proposed theory. By using equation (20), $\langle V_c^2\rangle$ has been computed, and is compared with experimental results in Figure 7. Theoretical predictions for three values of frequency-invariant dissipation loss factor $\eta_s=\eta_c$ are given since the choice of structural damping seems to be critical for SEA. It can be seen from Figure 7 that the experimental data are approximately bounded by $\eta_s=0{\cdot}0003$ and $\eta_s=0{\cdot}03$, which are typical values for a lightly damped structure. It is possible that η_s and η_c vary with frequency in the experiment; this is not included in our calculations. Accordingly, the agreement between theory and experiment is deemed to be excellent.

Further comparison between theory and experiment can be made for the case of a semi-infinite shaft considered in the example case II. By using equations (1), (7) and (8) for η_{sc}, the mobility levels were computed and found to be given by straight lines, as shown in Figure 8. These lines represent the asymptotic behavior of the system when the shaft is very long: i.e., $L_s\to\infty$. Again, most experimental data are bounded within the range given by $\eta_s=0{\cdot}0003$ to $0{\cdot}03$. Next consider the finite shaft length $L_s=1{\cdot}32$ m of high modal density n_s. In Figure 9 the coupling loss factor η_{sc} for this compared with the result for a semi-infinite shaft. It can be seen that η_{sc} for the semi-infinite shaft follows the frequency-averaged values of the finite shaft. Finally, plate mobility levels predicted by SEA for these two cases are compared in Table 2 with the results yielded by the deterministic finite element model of Part II. Here, a nominal dissipation loss factor $\eta_s=\eta_c=0{\cdot}003$ was chosen for calculations. It is evident that SEA is indeed applicable for this physical system.

TABLE 2

Comparison of results for example case III

One-third octave band center frequency (Hz)	Plate mobility level (dB $re\langle V^2\rangle_{ref}=1{\cdot}0\ \text{m}^2/\text{N}^2\text{s}^2$)			
	Experiment [26]	Deterministic FEM method [2]	SEA prediction	
			Finite shaft	Semi-infinite shaft
400	−102	−105	−102	−89
500	−92	−96	−87	−91
630	−95	−94	−90	−93
800	−88	−97	−93	−95
1000	−87	−95	−97	−97
1250	−97	−108	−101	−100
1600	−108	−115	−106	−104
2000	−106	−107	−112	−106

6. CONCLUDING REMARKS

The vibration transmission through a bearing in a generic shaft-bearing-plate system has been analyzed by using the SEA technique. A new theoretical procedure has been developed to compute the frequency-averaged coupling loss factor which relies on the solution of the boundary value problem at the plate-bearing interface. This scheme incorporates the rolling element bearing stiffness matrix developed earlier as a part of the deterministic vibration models in the companion papers Parts I-III [1-3]. The proposed formulation has been applied to a physical set-up consisting of a shaft cantilevered to a plate through a bearing support. The vibratory response of the rectangular plate predicted by SEA has been found to be in good agreement with measurements and with the results of the deterministic models of Part II. There are still several unresolved issues which require further research. For example, a more precise analysis of the moment applied to a plate through a beam in example case I is required. Improved estimation procedures for damping associated with bearing systems are needed. Perhaps of more importance is the extension of proposed methodology to rotating machinery noise and vibration problems. In fact, work is in progress with application to the gearboxes.

ACKNOWLEDGMENT

We wish to thank the NASA Lewis Research Center for supporting this research at The Ohio State University, and J. S. Lin and D. R. Houser for providing the experimental data of case III.

REFERENCES

1. T. C. LIM and R. SINGH 1990 *Journal of Sound and Vibration* **139**(2), 179-199. Vibration transmission through rolling element bearings, part I: bearing stiffness formulation.
2. T. C. LIM and R. SINGH 1990 *Journal of Sound and Vibration* **139**(2), 201-225. Vibration transmission through rolling element bearings, part II: system studies.
3. T. C. LIM and R. SINGH 1991 *Journal of Sound and Vibration* **151**(1), 31-54. Vibration transmission through rolling element bearings, part III: geared rotor system studies.
4. R. H. LYON 1975 *Statistical Energy Analysis of Dynamical Systems.* Cambridge, Massachusetts: The MIT Press.
5. J. WOODHOUSE 1981 *Applied Acoustics* **14**, 455-469. An introduction to statistical energy analysis of structural vibration.
6. R. H. LYON and E. EICHLER 1964 *Journal of the Acoustical Society of America* **36**(7), 1344-1354. Random vibration of connected structures.
7. R. H. LYON and T. D. SCHARTON 1965 *Journal of the Acoustical Society of America* **38**(2), 253-261. Vibrational-energy transmission in a three-element structure.
8. R. S. LANGLEY 1989 *Journal of Sound and Vibration* **135**, 499-508. A general derivation of the statistical energy analysis equations for coupled dynamic systems.
9. E. H. DOWELL and Y. KUBOTA 1985 *Journal of Applied Mechnics* **52**, 949-957. Asymptotic modal analysis and statistical energy analysis of dynamical systems.
10. Y. KUBOTA and E. H. DOWELL 1986 *Journal of Sound and Vibration* **106**, 203-216. Experimental investigation of asymptotic modal analysis for a rectangular plate.
11. Y. KUBOTA, H. D. DIONNE and E. H. DOWELL 1988 *Journal of Vibration, Acoustics, Stress, and Reliability in Design* **110**, 371-376. Asymptotic modal analysis and statistical energy analysis of an acoustic cavity.
12. E. SKUDRZYK 1980 *Journal of the Acoustical Society of America* **67**(4), 1105-1135. The mean-value method of predicting the dynamic response of complex vibrators.
13. V. R. MILLER 1980 *M.S. Thesis, The Ohio State University.* Prediction of interior noise by statistical energy analysis (SEA) method.
14. B. L. CLARKSON and K. T. BROWN 1985 *Journal of Vibration, Acoustics, Stress, and Reliability in Design* **107**, 357-360. Acoustic radiation damping.

15. J. C. SUN, H. B. SUN, L. C. CHOW and E. J. RICHARDS 1986 *Journal of Sound and Vibration* **104**, 243–257. Predictions of total loss factors of structures, part II: loss factors of sand-filled structure.
16. G. J. STIMPSON, J. C. SUN and E. J. RICHARDS 1986 *Journal of Sound and Vibration* **107**, 107–120. Predicting sound power radiation from built-up structures using statistical energy analysis.
17. A. J. KEANE and W. G. PRICE 1987 *Journal of Sound and Vibration* **117**, 363–386. Statistical energy analysis of strongly coupled systems.
18. P. J. REMINGTON and J. E. MANNING 1975 *Journal of the Acoustical Society of America* **57**(2), 374–379. Comparison of statistical energy analysis power flow predictions with an "exact" calculation.
19. J. WOODHOUSE 1981 *Journal of the Acoustical Society of America* **69**(6), 1695–1709. An approach to the theoretical background of statistical energy analysis applied to structual vibration.
20. P. W. SMITH, JR. 1979 *Journal of the Acoustical Society of America* **65**(3), 695–698. Statistical models of coupled dynamical systems and the transition from weak to strong coupling.
21. G. P. MATHUR, J. E. MANNING and A. C. AUBERT 1988 *NOISE-CON* 88, *Purdue University, West Lafayette.* Bell 222 helicopter cabin noise: analytical modeling and flight test validation.
22. J. L. GUYADER, C. BOISSON and C. LESUEUR 1982 *Journal of Sound and Vibration* **81**, 81–92. Energy transmission in finite coupled plates, part I: theory.
23. W. L. GHERING and D. RAJ 1987 *Proceedings of the Winter Annual Meeting of the American Society of Mechnical Engineers, Boston*, 81–90. Comparison of statistical energy analysis predictions with experimental results for cylinder-plate-beam structures.
24. I. DYER 1960 *Journal of the Acoustical Society of America* **32**(10), 1290–1296. Moment impedance of plates.
25. L. CREMER, M. HECKEL and E. E. UNGAR 1973 *Structure-Borne Sound.* Berlin: Springer-Verlag.
26. J. S. LIN 1989 *M.S. Thesis, The Ohio State University.* Experimental analysis of dynamic force transmissibility through bearings.

APPENDIX: LIST OF SYMBOLS

A_c	plate surface area
A_s	shaft cross-sectional area
c	wave speed
EI	flexural rigidity of the shaft
E_s, E_c	total vibratory energy level in the shaft-bearing (s) subsystem and plate (c) subsystem
$F_{ysa}(t)$	applied alternating shear force on the shaft
F_{ysm}	applied mean shear force on the shaft
$\{f\}_b$	bearing force vector
h_c	plate thickness
$[K]_{bm}$	proposed bearing stiffness matrix of dimension 6
k_{bij}	bearing stiffness coefficient, $i, j = x, y, z, \theta_x, \theta_y, \theta_z$
k_s, k_c	shaft (s) or plate (c) wavenumber
L_s	shaft length
M_{xsa}	alternating shaft bending moment about x direction
m_c	plate mass
m_s	shaft mass
n_c	plate modal density
n_s	shaft modal density
Re	real part of a complex number
t	time
$\langle V^2 \rangle$	spatially and frequency bandwidth averaged mean square mobility
v_{ysa}	alternating shaft tranverse velocity
$\{v\}_b$	bearing velocity vector
Z_c	driving point plate impedance at bearing junction
Z_s	driving point shaft impedance at bearing junction
Z_f	driving point shaft impedance at forcing location
η_s, η_c	dissipation loss factor for the shaft-bearing (s) or plate (c) subsystems
η_{sc}	coupling loss factor

κ radius of gyration
Π_s external power input to the shaft-bearing (s) subsystem
Π_{sc} net power transfer from the shaft-bearing (s) subsystem to plate (c) subsystems
ρ material density
ω bandwidth center frequency
$( )^*$ complex conjugate